Control of the Position of Oxygen Delivery in Soybean Lipoxygenase-1 by Amino Acid Side Chains within a Gas Migration Channel*

Lara Collazo[1] **and Judith P. Klinman**[2]

From the Department of Molecular and Cell Biology, Department of Chemistry, and the California Institute for Quantitative Biosciences (QB3), University of California, Berkeley, California 94720

Understanding gas migration pathways is critical to unraveling structure-function relationships in enzymes that process gaseous substrates such as O_2, H_2, and N_2. This work investigates the role of a defined pathway for O_2 in regulating the peroxidation of linoleic acid by soybean lipoxygenase 1. Computational and mutagenesis studies provide strong support for a dominant delivery channel that shuttles molecular oxygen to a specific region of the active site, thereby ensuring the regio- and stereospecificity of product. Analysis of reaction kinetics and product distribution in channel mutants also reveals a plasticity to the gas migration pathway. The findings show that a single site mutation (I553W) limits oxygen accessibility to the active site, greatly increasing the fraction of substrate that reacts with oxygen free in solution. They also show how a neighboring site mutation (L496W) can result in a redirection of oxygen toward an alternate position of the substrate, changing the regio- and stereospecificity of peroxidation. The present data indicate that modest changes in a protein scaffold may modulate the access of small gaseous molecules to enzyme-bound substrates.

Structure-function studies of enzymes have moved beyond an exclusive focus on active site protein side chains, with the growing recognition that distal residues can have a significant impact on catalytic bond cleavage events (1, 2). Topological features within the protein matrix, such as cavities and channels, can also play key roles in the flux of biomolecules. For proteins with gaseous substrates, *e.g.* O_2, H_2, N_2, and NH_3, specific channels have been proposed either to transport reactive intermediates between active sites within a multifunctional enzyme (3) or to guide these small molecules from the solvent to the active site. The likely importance of the latter is relevant to a wide range of enzymes that includes oxidases, monooxygenases, nitrogenases, and hydrogenases (4–17). The involvement of functionally evolved gas channels represents a significant departure from earlier held views in which random,

transient fluctuations within a protein were proposed to facilitate the delivery of gaseous substrates to their site of binding and/or reactivity.

Studies of lipoxygenases have aided in this shift in perception, given their requirement to capture O_2 via highly regio- and stereospecific pathways. As illustrated in Fig. 1 for the reaction catalyzed by soybean lipoxygenase-1 (SLO-1),[3] the delocalized nature of the free radical intermediate generated from the preferred substrate linoleic acid (LA) predicts that four unique products will be produced in equal amounts in solution. By contrast, native SLO-1 produces the 13S-hydroperoxide product (13S-HPOD) in greater than 90% yield for reaction of WT enzyme under optimal conditions. The precise mechanism by which SLO-1, as well as other lipoxygenases, maintain the regio- and stereospecificity of product peroxidation has engendered a variety of proposals that include: (i) an alteration in substrate binding (from head to tail first) as a means of reversing the enantiomeric specificity of O_2 addition to a fixed carbon center; (ii) the interchange of a single active site residue between Gly and Ala to alter the position (but not the face) of O_2 attack; and (iii) a directed movement of O_2 through the protein matrix toward a spatially defined position of substrate that is capable of simultaneously controlling both the position and face of O_2 attack on a substrate-derived free radical intermediate (4, 16, 18).

Although all three of the above factors may play a role in the evolution of lipoxygenases that catalyze the formation of stereo- and regiochemically distinct hydroperoxides, there remains the generic question of how each enzyme manages a transit of O_2 from bulk solvent toward the reactive carbon of buried substrate. The x-ray structure of SLO-1 is quite informative in this regard, implicating a putative gas channel that appears "crimped" in its middle at the residue Ile[553] (18). Earlier support for the involvement of this channel came from the generation of an I553F mutant enzyme that showed a reduction in rate for the O_2-dependent portion of the SLO-1 reaction accompanied by only a modest impact on the initial C–H abstraction step and the position/stereochemistry of substrate peroxidation (3). The reaction mechanism invoked for I553F involves protein breathing modes capable of relieving a mutation-induced "steric impasse" toward O_2 (19). In the present

[1] Present address: Genentech, Inc., One DNA Way, South San Francisco, CA 94080.
[2] To whom correspondence should be addressed. Tel.: 510-642-2668; Fax: 510-643-4500; E-mail: klinman@berkeley.edu.

[3] The abbreviations used are: SLO-1, soybean lipoxygenase-1; LA, linoleic acid; HPOD, hydroperoxyoctadecadienoic acid; ILS, implicit ligand sampling; HODE, hydroxyoctadecadienoic acid.
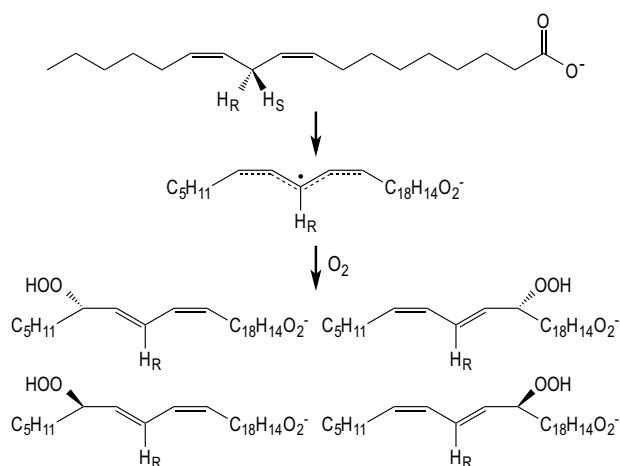
FIGURE 1. **Simplified chemical mechanism of SLO illustrating two half-reactions in which the C–H bond is cleaved at carbon 11, and O₂ is inserted at carbon 13.** The primary 13S-HPOD product is shown as the *upper left hand* product structure, whereas reaction in solution is predicted to produce a mixture of two 13-HPOD and two 9-HPOD products.

study, we have greatly extended this line of inquiry via the incorporation of a range of amino acid side chains into four targeted channel positions. The new findings both corroborate a role for a discrete gas channel in SLO-1 while revealing conditions capable of altering the pathway for O_2 delivery to the active site of lipoxygenases.

Experimental Procedures

Identifying Pathways for O_2 Migration—The CAVER 3.0 software tool was employed to identify all possible routes from the active site in SLO to the solvent, based on the x-ray coordinates of the enzyme and a radius for gas migration (18, 20). To approximate the location of the active site, starting point coordinates within SLO were computed as the spatial averages of the coordinates of the catalytic iron atom and active site residue Leu[546]. A minimum bottleneck radius of 0.9 Å was specified. The results were visualized in the molecular visualization program VMD to facilitate comparison to implicit ligand sampling (ILS) results (21).

Mapping O_2 Affinity in SLO—The LEaP module of the Amber 11 software package was used to generate a fully solvated model of SLO based on the x-ray coordinates of the enzyme (18, 22). In the crystal structure, the nonheme iron is in the ferrous state, complexed by the side chains of His[499], His[504], His[690], and Asn[694] in addition to the carboxylate of Ile[839] and a water molecule (18). Topology and force field parameters for the bound water in the active site were adapted from a TIP3P model, and parameters for the iron ligand were adapted from those published for a six-coordinate iron in a heme-containing protein (23, 24). Amber FF99 force field parameters were employed for the protein, as in previous SLO simulations (25–27). The SLO structure was solvated in a truncated octahedral box of TIP3P waters, and the overall charge of the system was neutralized by the addition of 11 peripheral sodium cations (26). After equilibration, a 10-ns molecular dynamics simulation of the SLO system was performed using an isothermic-isobaric ensemble, as is required for ILS analysis (28).

The ILS tool was applied to the molecular dynamics simulation of SLO to assess regions favorable for oxygen migration within the enzyme. The ILS technique allows for the generation of a three-dimensional map of the Gibbs free energy cost, or $\Delta G_s(O_2)$, associated with transferring an oxygen molecule from a vacuum to a particular position inside the protein (28). $\Delta G_s(O_2)$ was evaluated for every 1 Å^3 volume element throughout the SLO system. Within each of these elements, oxygen was placed in 20 different rotational orientations at each of 27 different positions on a $3 \times 3 \times 3$ grid. Five thousand protein conformations were sampled from the 10-ns trajectory. A three-dimensional free energy map was generated describing the distribution of oxygen throughout SLO. Regions of the enzyme likely to be occupied by oxygen were identified by drawing isoenergy surfaces—that is, plotting all points in a protein for which the $\Delta G_s(O_2)$ is below a certain value. The results were visualized in VMD, the molecular visualization program in which the ILS method is realized (21).

Site-directed Mutagenesis and Protein Expression and Purification—Seven SLO mutants were generated through site-directed mutagenesis according to the QuikChange II protocol (Agilent Technologies). HPLC-purified primers were purchased from Eurofins MWG Operon, and sequencing was performed by UC Berkeley Sequencing Facility. The V564F lipoxygenase mutant was expressed and purified using the SLO pT7-7 plasmid in *Escherichia coli*, as described previously (29, 31). WT SLO and all other mutants were expressed and purified as His tag fusion proteins using the SLO pET-30Xa/LIC plasmid, acquired from Professor Betty Gaffney at Florida State University. These enzymes were expressed and purified as described previously, with several modifications (31). His-tagged SLO was eluted with wash buffer containing 250 mM imidazole and dialyzed overnight (4 °C) into 20 mM Bis-Tris (pH 6.6) buffer. The dialyzed eluate from nickel-nitrilotriacetic acid chromatography was concentrated and injected onto an FPLC system with a 6-ml UNO S6 column (Bio-Rad) for separation by cation exchange chromatography. A salt gradient for protein elution was run from 0.0 to 0.5 M NaCl in 20 mM Bis-Tris (pH 6.6) buffer. SLO activity was assayed in fractions by monitoring the formation of HPOD at 234 nm upon the addition of 5 μl of a column fraction to 245 μl of 100 μM linoleic acid in 0.1 M borate (pH 9.0). Fractions containing SLO activity were combined, dialyzed into 0.1 M borate (pH 9.0), concentrated, and stored at −80 °C.

Enzyme Kinetics—Oxygen electrode and UV kinetic assays were performed for WT SLO and each mutant lipoxygenase as described previously (19, 29, 31). Oxygen concentration was varied from 30 to 1365 μM. LA concentration was varied from 2 to 80 μM. All kinetic assays were performed at 20 °C and in 0.1 M borate (pH 9.0). Reported estimates of k_{cat} are derived from oxygen electrode studies rather than UV kinetic data, allowing extrapolation rather than correction for saturating O_2.

Enzyme Regio- and Stereospecificity—The reactions were incubated at 20 °C in 0.1 M borate (pH 9.0) and 100 μM LA for 5 h after initiation with enzyme. The reactions at elevated and depressed O_2 concentrations were performed using a Clark-type electrode from Yellow Springs Inc. and a YSI-5300 biological oxygen monitor. The reaction mixtures were quenched at
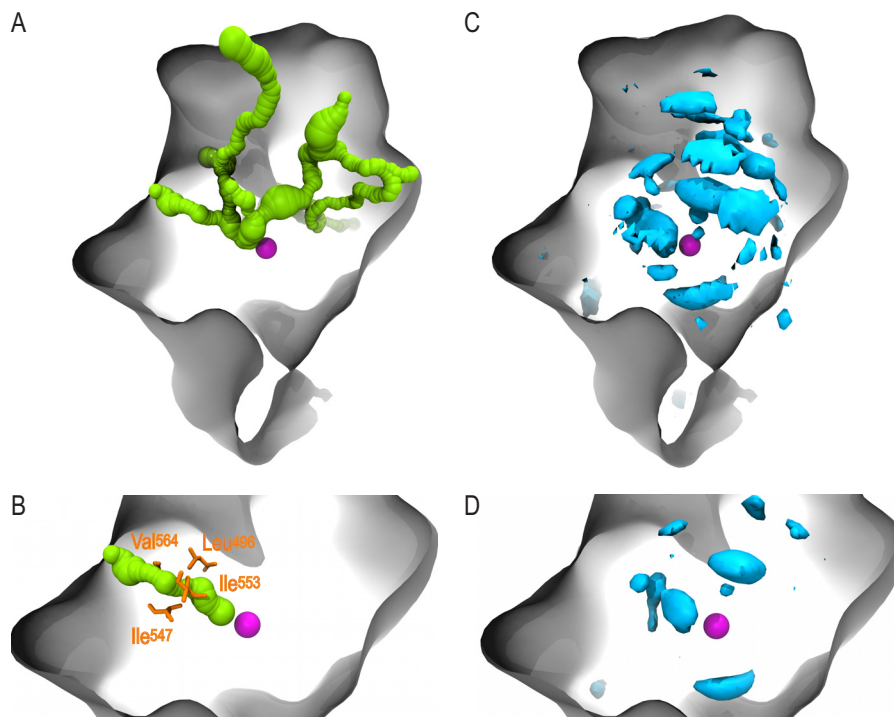
FIGURE 2. *A* and *B*, computational analysis of O_2 transport in SLO using CAVER. The surface of SLO is depicted in *gray*, and the catalytic iron, a hallmark of the active site, is represented as a *magenta sphere*. *A*, eight channels (*green*) were detected extending from the buried active site in SLO to the exterior of the protein. *B*, channel A (*green*) was identified as the most favorable route from the active site to the solvent according to a throughput metric computed by CAVER that favors short, wide channels. Residues within 1.5 Å of the bottleneck of channel A are depicted in *orange* and are listed here, sorted from closest to the iron center: Ile[553], Ile[547], Leu[496], and Val[564]. *C* and *D*, computational analysis of O_2 transport in SLO using ILS. SLO is represented by a *gray surface*, and the catalytic iron atom is depicted as a *magenta sphere*. *C*, the -0.5 kT isoenergy surface (*cyan*) highlights multiple, preferred pockets for oxygen to inhabit throughout the SLO protein matrix. *D*, the -2.5 kT isoenergy surface (*cyan*) imposes a more stringent requirement than the -0.5 kT surface, including only the most favorable regions for oxygen migration in the protein matrix. Note the pocket to the *left* of the catalytic iron, which is located closest to the active site.

pH 4 (glacial acetic acid) and extracted into dichloromethane. Reaction products were taken to dryness under a stream of N_2 and stored at -80 °C until HPLC analysis. Reaction products were injected onto a reverse phase HPLC system with a Luna C18 5-μm column (0.46 × 25 cm; Phenomenex). An isocratic solvent system of 78% methanol and 21.9% water with 0.1% acetic acid was employed to elute HPOD. A flow rate of 0.9 ml/min was used. HPOD was collected, taken to dryness under N_2, and reduced via incubation for >1 h with a solution of 1.9 m$_M$ triphenylphosphine in methanol. The hydroxyoctadecadienoic acid (HODE) generated was taken to dryness under N_2 and stored at -80 °C until chiral phase HPLC analysis.

HODE was injected onto a chiral phase HPLC system with a Chiralcel OD-3 column (0.46 × 25 cm; Chiral Technologies, Inc.). An isocratic solvent system of 1.55% isopropanol, 0.3% acetic acid, and 98.2% hexanes was employed to separate the 13*S*, 13*R*, 9*S*, and 9*R* isomers. A flow rate of 2 ml/min was used. Assignment of the four HODE isomeric peaks was accomplished using standards of 13*S*-, 13*R*-, 9*S*-, and 9*R*-HODE acquired from Cayman Chemical.

Results

Computational Prediction of the Preferred Route(s) for Oxygen Delivery to the SLO-1 Active Site—Two parallel computational techniques, CAVER and implicit ligand sampling, were employed to probe gas migration within SLO-1. The CAVER 3.0 software tool was used to identify pathways linking the SLO active site to the solvent. Assigning a bottleneck radius of 0.9 Å

for passage of O_2 through the protein, eight routes were detected (Fig. 2*A*) with the length, average radius, and minimum radius, summarized in Table 1. Pathways were also ranked from most favorable (A) to least favorable (H) by CAVER, based on a throughput parameter that takes into account channel length as well as width. Channel A (Fig. 2*B*) was identified by CAVER as the most favorable route for oxygen to travel from the solvent to the active site. This channel exhibits the highest throughput (0.4) and largest bottleneck radius (1.1 Å), as well as the second largest mean radius and second shortest total length. Four residues were identified within 1.5 Å of the bottleneck of channel A: Ile[553], Ile[547], Leu[496], and Val[564] (Fig. 2*B*). In short, our analysis indicates that although multiple pathways link the buried SLO active site and solvent, channel A is identified as the preferred route for oxygen delivery to the site of catalysis.

In parallel with the geometric algorithm employed by CAVER, ILS simulations were performed to detect energetically favorable regions for oxygen to occupy within SLO. This technique infers gas migration pathways by generating a three-dimensional map of the Gibbs free energy cost associated with placing an oxygen molecule anywhere in the protein. Lower free energy values are associated with a greater probability of finding oxygen. Regions of SLO likely to be occupied by oxygen were mapped by drawing free energy isosurfaces at -0.5 kT (Fig. 2*C*) and -2.5 kT (Fig. 2*D*). Together, these energy maps indicate that although pockets favorable for the gas exist

TABLE 1

Characterization of eight channels detected and ranked by CAVER

Length, mean radius, and bottleneck radius were computed by the program in addition to a throughput parameter that reflects the overall competency of each channel. Based on this throughput parameter, each channel was ranked by CAVER, with A representing the most favorable tunnel and H representing the least favorable path. Pathways with small lengths and large radii (e.g. A) were preferred to longer, narrower tunnels (e.g. H).

	A	B	C	D	E	F	G	H
Length (Å)	21	20	25	41	50	44	109	133
Mean radius (Å)	1.6	1.4	1.5	1.8	1.5	1.4	1.3	1.3
Bottleneck radius (Å)	1.1	0.9	1	0.9	0.9	1	0.9	0.9
Throughput	0.4	0.3	0.3	0.2	0.1	0.1	0.002	0.0003

FIGURE 3. **SLO depicted with the −2.5 kT isoenergy surface computed by ILS, as well as channel A and its bottleneck residues identified by CAVER.** The largest pocket outlined by the −2.5 kT isoenergy surface (*cyan*) directly overlaps with channel A (*green*), the top-ranked channel detected by CAVER. This region is also in close proximity to the bottleneck residues identified by CAVER (*orange*), highlighting the accordance of these two techniques. Overlap of the −2.5 kT isoenergy surface with other channels detected by CAVER (B–H) is comparatively small, consistent with channel A representing the biologically relevant pathway.

throughout SLO, dioxygen tends to concentrate near the active site. Interestingly, the largest pocket outlined by the −2.5 kT isosurface directly overlaps with the top-ranked pathway identified by CAVER, channel A (Fig. 3). This pocket, which is adjacent to the active site, is also located in close proximity to the four bottleneck residues of channel A. Together, energetic and geometric insights from ILS and CAVER, respectively, point to a single pathway for oxygen delivery and implicate four residues in modulating oxygen access to the active site.

Introducing Larger Amino Acid Side Chains into Channel A Disrupts Oxygen Trafficking, as Evidenced by Altered Kinetic Parameters for O_2—To assess the functional role of channel A, steric bulk was introduced at bottleneck residues 553, 547, 496, and 564 via site-directed mutagenesis. The impact of mutations on oxygen delivery was assessed by determining k_{cat}, $K_m(O_2)$, $K_m(LA)$, and the respective k_{cat}/K_m parameters (Table 2). Focusing on the insertion of Trp at the four positions, the change in $k_{cat}/K_m(LA)$ is negligible for positions 547 and 564 in relation to WT. By contrast, Trp at positions 553 and 496 leads to quite significant changes in $k_{cat}/K_m(LA)$, with values that are only 10^{-3} to 10^{-2} of WT. In the case of $k_{cat}/K_m(O_2)$, all of the selected mutants indicate rate reductions, ranging from 2-fold (V564W) to ~10^4-fold (I553W). This behavior is mirrored in K_m values of 132–744 μM O_2 compared with 38 μM for WT SLO. A key issue is the degree to which an increase in side chain size decreases $k_{cat}/K_m(O_2)$ to a greater extent than $k_{cat}/K_m(LA)$. This feature is evaluated in the final column of Table 2, highlighting the largest impact of Trp occurring at positions 553 and 496 on O_2. In support of a straightforward analysis of the observed $K_m(O_2)$ and $k_{cat}/K_m(O_2)$ parameters, we note the absence of an elevation of the $K_m(LA)$ for any of the variants interrogated here. All previous studies of mutants of SLO-1 (*cf.* Refs. 29, 30, and 32) support an unchanged rate determining step that is controlled by C–H cleavage, implying that $K_m \cong K_d$ for both WT and mutant variants. The consequences of Trp at positions 553 and 496 become even more apparent following analysis of the product distribution among the four possible HPODs (*cf.* Fig. 1).

Diminishing O_2 Availability at the Active Site of WT SLO-1 Disrupts the Regio- and Stereospecificity of Product—In addition to kinetic parameters, the regio- and stereospecificity of the SLO-catalyzed reaction provides a measure of oxygen availability at the active site. Significant loss of regiospecificity, for example, has been documented in the reaction of LA with SLO under low oxygen conditions, where the ratio of 13 HPOD to 9 HPOD approaches 1:1 (33). Diminished oxygen availability is
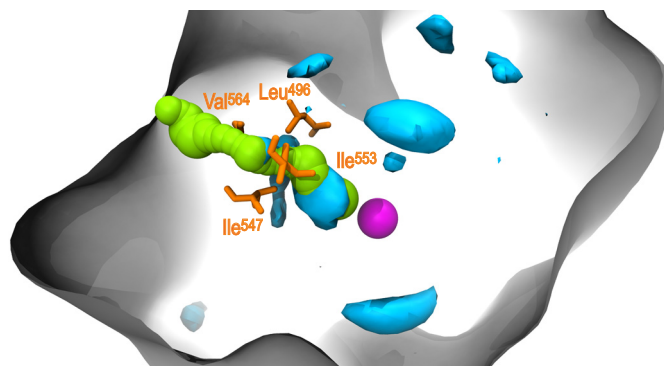
thought to result in increased dissociation of the linoleyl radical intermediate into solution, where it can react indiscriminately with oxygen. Our investigation of the SLO-catalyzed reaction at low oxygen confirms previous findings with respect to regiospecificity and furthermore discerns the proportion of 13*S*-, 13*R*-, 9*R*-, and 9*S*-HPOD produced at low O_2 (Fig. 4). At ambient oxygen, 13*R*-, 9*S*-, and 9*R*-HPOD are present in small amounts and account in total for <10% of HPOD produced. At 28 μM O_2, by contrast, a substantial amount of 13*R*-, 9*S*-, and 9*R*-HPOD is generated. The alternate isomers are produced in approximately equivalent amounts, each accounting for ~21% of total HPOD produced. These results support the hypothesis that reduced oxygen availability leads to nonspecific oxygen insertion during the peroxidation of LA by SLO and serve as controls for the impact of site-specific mutagenesis and altered oxygen tension on product distribution.

Introducing Steric Restriction into Channel A Disrupts the Regio- and Stereospecificity of Product HPODs—The impact of mutation on SLO-1 regio- and stereospecificity provides one important probe of the disruption of oxygen trafficking. This is seen to be most dramatic for three SLO mutants, I553W, L496F, and L496W (Table 3). In accordance with the kinetic data (Table 2), analysis of product distribution implicates important roles for positions 553 and 496 in directing O_2 from the solvent to the correct position and face within the substrate-derived pentadienyl radical.

Replacement of Ile[553], which is fully conserved in all soybean lipoxygenases, by Trp and reaction with LA produces 45% 13*S*-HPOD, whereas the WT enzyme generates 93% 13*S*-HPOD. A substantial amount of 13*R*-, 9*S*-, and 9*R*-HPOD is thus produced with I553W. These isomers account for >50% of HPOD and, importantly, are seen to be generated in roughly equivalent amounts. The regio- and stereospecificity of the I553W mutant resembles that of the WT reaction at low O_2, consistent with restricted oxygen availability and the resulting increased dissociation of the linoleyl radical to solution. This explanation is supported by the significantly elevated $K_m(O_2)$ determined for this mutant (744 μM O_2). We note that introducing phenylala-

TABLE 2

Kinetic characterization of SLO mutants

The experiments were conducted at 20 °C, pH 9. k_{cat} is at saturating concentrations of both LA and O_2, whereas the k_{cat}/K_m indicated is at saturation with regard to the alternate substrate.

SLO	k_{cat}	K_m		k_{cat}/K_m		Impact of mutation on k_{cat}/K_m[a]
		LA	O_2	LA	O_2	
	s^{-1}	μM	μM	$s^{-1}\,\mu M^{-1}$	$s^{-1}\,\mu M^{-1}$	
WT[b]	211 ± 9 (230 ± 15)	20 ± 2 (18 ± 3)	38 ± 5 (31 ± 3)	11 ± 1	6 ± 1	
I553F[c]	102 ± 8	19 ± 4	142 ± 58	5 ± 1	0.7 ± 0.3	3.8
I553W	0.40 ± 0.04	25 ± 5	744 ± 142	0.016 ± 0.004	0.0005 ± 0.0001	18
I547F	66 ± 5	3.0 ± 0.3	44 ± 11	22 ± 3	1.5 ± 0.4	8
I47W	44 ± 2	5.0 ± 0.5	50 ± 7	9 ± 1	0.9 ± 0.1	5.5
L496F	44 ± 3	5 ± 1	132 ± 26	9 ± 2	0.3 ± 0.1	16
L496W	1.6 ± 0.1	11.0 ± 0.8	171 ± 33	0.15 ± 0.01	0.009 ± 0.002	9.1
V564F	60 ± 1	6.0 ± 0.4	46 ± 5	10 ± 1	1.3 ± 0.1	4.2
V564W	99 ± 5	8.0 ± 0.7	32 ± 6	12 ± 1	3 ± 1	2.2

[a] The impact of mutation for the k_{cat}/K_m for either LA or O_2 was first calculated. The ratio of the mutational impairment on k_{cat}/K_m for O_2 relative to that for LA is reported in the final column.

[b] The numbers in parentheses indicate the measured parameters with non-His-tagged protein. As a frame of reference, native SLO-1, isolated from soybeans, gave $k_{cat} \cong 150$ s^{-1}, $K_m(LA) \cong 40$ μM, and $K_m(O_2) \cong 30$ μM under the same reaction conditions (37).

[c] The data for I553F are from Ref. 19.
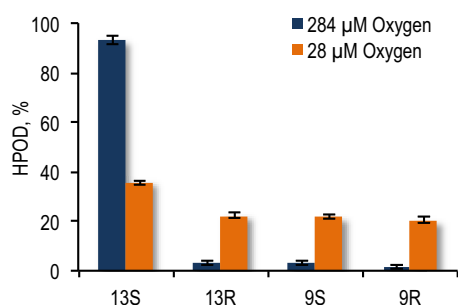

FIGURE 4. **Impact of diminished O_2 on the regio- and stereospecificity of WT-SLO-1.**

TABLE 3

Regio- and stereospecificity of product formation with mutant forms of SLO-1

The experiments were performed under the conditions of pH 9, 20 °C, and ambient O_2 concentration (284 μM). The errors range from 6 to 18% of the stated values.

SLO	13S HPOD	13R HPOD	9S HPOD	9R HPOD
	%	%	%	%
WT	93	3	3	2
I553F[a]	95	2	1	2
I553W	45	16	22	17
I547F	93	2	2	2
I547W	93	2	3	2
L496F	63	9	14	14
L496W	32	10	29	30
V564F	89	2	4	5
V564W	86	3	5	5

[a] Ref. 4.

nine at position 553 does not disrupt regio- and stereospecificity in the same way as tryptophan. Despite exhibiting an elevated $K_m(O_2)$, the I553F mutant produces >90% 13S-HPOD. The introduction of phenylalanine at position 553 reduces the rate at which O_2 reaches the substrate derived radical (19) while leaving the regio- and stereospecificity of product formation intact. We propose that the key factor in determining the fidelity of product formation is the ratio of rate constants for trapping of the bound pentadienyl intermediate by O_2 *versus* its release from enzyme. The insertion of Trp at position 553 has clearly tipped the balance toward a solution-based reaction of substrate with O_2, in a manner resembling the impact of reduced O_2 concentration on the product distribution of WT enzyme.

Regio- and stereospecificity is also dramatically disrupted in the reaction of both Leu[496] mutants with LA. Reaction with the phenylalanine and tryptophan mutants produces 63 and 31% 13S-HPOD that is accompanied by a substantial amount of 13R-, 9S-, and 9R-HPOD; together, these alternate isomers account for 37 and 69% of HPOD produced in reactions with L496F and L496W (Table 3). It is significant that the 13R, 9S, and 9R isomers are produced in unequal amounts, contrasting with the behaviors of WT SLO at low oxygen and the I553W mutant. This is particularly apparent for the L496W mutant, where the 9S and 9R isomers each account for 29 and 30% of HPOD produced compared with 10% for the 13R isomer. The disparity is more subtle in the case of L496F, where the 9S and 9R isomers account for 14% of HPOD produced compared with 9% for 13R-HPOD. We conclude that the altered regio- and stereospecificity of the Leu[496] mutant reactions cannot be simply explained by a restricted availability of O_2 at the active site that results in increased loss of the substrate radical to solvent. Rather, the elevated amount of 9R and 9S-HPOD suggests a gain of function for the Leu[496] mutations, *i.e.* the opening up of an alternate route for gas migration that allows O_2 to access carbon 9 of the substrate radical. We note that earlier studies (31) have discussed a changeover from the production of 13S- to 13R-HPOD products in the event of a "reverse binding" of substrate, under conditions where the fatty acid carboxylate of substrate becomes protonated and can orient itself toward the protein interior. Whereas this phenomenon may account for behaviors at pH 7, it is an unlikely explanation for the behavior reported herein at pH 9. With the expectation that reverse binding will not be sensitive to increased O_2 levels and to further test out the hypothesis that the behavior of the Ile[553] and Leu[496] variants is due to perturbations in a gas channel, we examined the impacts of O_2 concentration on product distributions with I553W and L496W.

Increased Levels of [O_2] Partially Rescue WT Regio- and Stereospecificity in Reactions of I553W and L496W—Reaction of both the I553W and L496W mutants was characterized at elevated O_2 concentration (1365 μM O_2). As shown in Fig. 5, increasing [O_2] from 284 to 1365 μM reduces the amount of 13R, 9S, and 9R isomers generated by the I553W mutant from 55 to 35% of total HPOD produced. The amount of 13S-HPOD
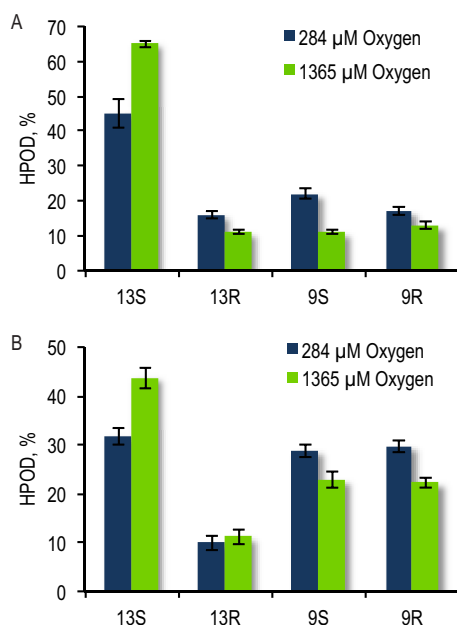
FIGURE 5. **Impact of increasing O$_2$ concentration on the product distribution for reaction of I553W (*A*) and L496W (*B*) SLO with LA.**

generated by the I553W reaction similarly increases from 45% at ambient O$_2$ to 65% at 1365 μM O$_2$. Increased O$_2$ can be concluded to partially restore the regio- and stereospecificity of this mutant reaction, indicating that additional O$_2$ compensates for impaired oxygen delivery in the mutant.

Elevated O$_2$ is also able to partially restore the regio- and stereospecificity of the L496W mutant reaction (Fig. 5), but not by uniformly decreasing the amount of 13*R*, 9*S*, and 9*R* isomers produced as seen for I553W. This observation indicates that increasing [O$_2$] has an impact that goes beyond simply increasing oxygen availability in relation to radical dissociation, as observed for I553W at high O$_2$. As noted earlier, a decrease in radical dissociation would affect the formation of the 13*R*, 9*S*, and 9*R* product isomers equally. In contrast, elevated [O$_2$] in L496W influences the partitioning of O$_2$ between oxygen transport pathways, reducing the reaction at carbon 9 and increasing product formed via the pathway leading to a reaction at carbon 13. This result strongly supports the conclusion of a higher barrier for O$_2$ reactivity through the normal channel (that leads to carbon 13) than for the newly introduced channel (leading to carbon 9) in L496W.

Discussion

Enzymes are complex systems that contain a variety of pockets, clefts, and channels throughout the protein matrix. These internal structural features can play an essential role in tuning enzyme function by modulating the flux of small molecules within the protein. For example, in flavo-monooxygenases and oxidases, oxygen delivery channels have been shown to guide oxygen from the solvent through preorganized protein cavities and direct it to the reacting C4a atom of the flavin cofactor (14, 34). In 12/15 lipoxygenase, a preferred route for oxygen travel has been identified that links the solvent and buried active site (6). Similarly, crystallographic and computational studies have also implicated oxygen access paths in cyclooxygenase, copper

amine oxidase, cholesterol oxidase, and cytochrome *c* oxidase (8, 10, 11). The nuanced role of the protein matrix in influencing catalysis is not restricted to oxygen delivery. In hydrogenases, gas channels have been reported to selectively filter molecules such as oxygen and carbon monoxide to prevent inactivation at the active site (12, 17, 35). Recent investigation of heme nitric oxide/oxygen binding domains has suggested that tunnels not only direct gases to the heme iron but also modulate reversible gas binding (16). Importantly, our work is the first to directly implicate an oxygen channel in regulating regio- and stereospecificity by explicitly showing the production of alternate product isomers upon obstruction of the channel.

Lipoxygenases provide an ideal context in which to examine oxygen migration because product positional and stereochemistry, in addition to reaction kinetics, can report on oxygen targeting to the active site (36). In this work, the functional role of oxygen migration pathways was examined in SLO-1, the best studied member of the lipoxygenase family. Our computational and experimental findings support a role for a single delivery channel within SLO-1 that shuttles oxygen to the active site and ensures its regio- and stereospecific insertion during catalysis.

To examine oxygen trafficking within SLO-1 from both a structural and energetic perspective, two computational approaches were employed in parallel. ILS was used to identify regions favorable for oxygen travel throughout the protein whereas CAVER was employed to visualize pathways leading continuously from the active site to the exterior of the protein. Although these tools identify multiple pockets and pathways throughout the enzyme (Fig. 2), both converge on a single channel deemed most competent for oxygen delivery (Fig. 3) (20, 28) Interestingly, this channel is consistent with a cavity originally identified in the crystal structure of SLO and previously proposed as an O$_2$ channel (4, 18, 32).

The functional role of this putative oxygen pathway was confirmed by introducing steric bulk at its bottleneck residues via site-directed mutagenesis. Introducing tryptophan at positions 553 and 496, in particular, dramatically disrupts oxygen trafficking to the active site, as evidenced by alterations in Michaelis constants and $k_{cat}/K_m(O_2)$ (Table 2) and reaction regio- and stereospecificity (Table 3) that, importantly, is dependent on the exogenous O$_2$ level (Fig. 5). These observations point to a role for these residues as gatekeepers of a channel that shuttles oxygen to the active site.

Examining the regio- and stereospecificity of the I553W and L496W mutant reactions further reveals that introducing steric restriction at these positions disrupts oxygen trafficking in different ways. Tryptophan at position 553 diminishes oxygen availability at the SLO active site, effectively starving the enzyme for oxygen. Accordingly, the I553W reaction exhibits impaired regio- and stereospecificity similar to the reaction of WT SLO-1 at low oxygen (Table 3 and Fig. 4). This observation, coupled with the 20-fold increase in $K_m(O_2)$ for the I553W mutant, is proposed to reflect limited oxygen availability at the active site and increased dissociation of the linoleyl free radical intermediate into solution that then undergoes reaction with O$_2$ in a random manner. Consistent with this hypothesis, performing the I553W mutant reaction at high [O$_2$] partially res-
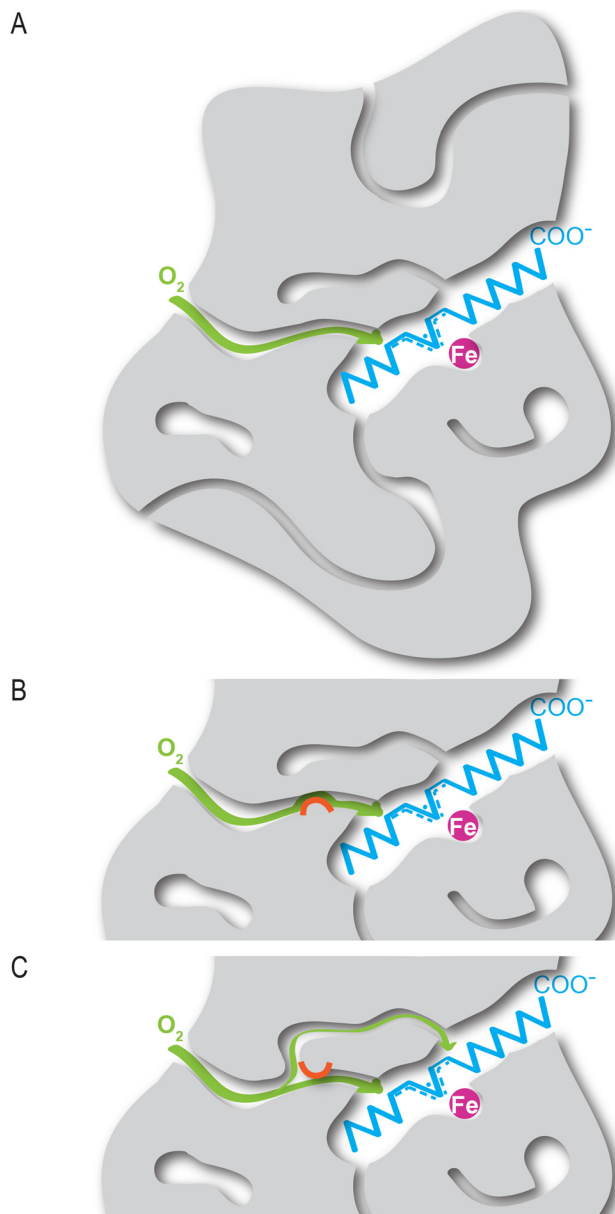
FIGURE 6. Model of gas (O_2) migration (*green*) in WT (*A*), I553W (*B*), and L496W SLO (*C*) based on computational and experimental studies. The SLO protein matrix is depicted in *gray*, LA is in *blue*, and the catalytic iron is in *magenta*. The *orange* semicircle represents positions of blockages.

cues the WT regio- and stereospecificity of the reaction (Fig. 5*A*).

Inserting tryptophan at position 496 has a more modest impact on oxygen availability at the active site, as evidenced by the changes in $k_{cat}/K_m(O_2)$ and $K_m(O_2)$ (Table 2). The unique feature of L496W is its impact on regio- and stereospecificity, revealing the creation of an alternate pathway to the active site that grants oxygen access to carbon 9 of the substrate-derived radical. Accordingly, the proportion of 9*S*- and 9*R*-HPOD generated increases dramatically in the L496W reaction with LA compared with WT SLO, whereas the proportion of 13*R*-HPOD increases to a much smaller extent (Table 3). Based on implicit ligand sampling analysis (Fig. 2), multiple regions favorable for oxygen binding exist proximal to the active site.

One or more of these regions may be rendered functional in the Leu[496] mutant enzymes.

Consistent with our experimental and computational findings, a model for gas migration in WT SLO, as well as the I553W and L496W mutants, is depicted in Fig. 6. Although the SLO protein matrix contains a variety of tunnels and cavities, one pathway is primarily utilized for oxygen delivery to the active site of the WT enzyme. This oxygen delivery channel becomes impaired in the I553W mutation (Fig. 6*B*). Accordingly, O_2 availability at the active site is diminished, as evidenced by the large decrease in $k_{cat}/K_m(O_2)$, an increased Michaelis constant for oxygen, and an increased proportion of equal levels of 13*R*-, 9*S*-, and 9*R*-HPOD produced in the peroxidation of LA that is partially reversed at elevated O_2 concentration. The L496W mutation, by contrast, appears to unlock an alternate pathway to the active site (Fig. 6*C*), significantly increasing the proportion of 9*S*- and 9*R*-HPOD produced in the peroxidation of LA in an O_2-dependent manner. These new findings, which extend previous evidence for a gas channel in SLO-1 (4), may provide insight into mechanisms for altered positions of oxygen delivery with the larger lipoxygenase family, as well as offer guidelines for the *de novo* design of enzymes that require gaseous molecules as cosubstrates.

Author Contributions—L. C. performed the experiments. J. P. K. and L. C. designed the experiments and wrote the manuscript.

References

1. Lee, J. 1., and Goodey, N. M. (2011) Catalytic contributions from remote regions of enzyme structure. *Chem Rev.* **111,** 7595–7624
2. Brodkin, H., DeLateur, N., Somarowthu, S., Mills, C., Novak, W., Beuning, P., Dagmar Ringe, and Ondrechen, M. (2015) Prediction of distal residue participation in enzyme catalysis. *Protein Sci.* **24,** 762–778
3. Mullins, L. S., and Raushel, F. M. (1992) Channeling of ammonia through the intermolecular tunnel contained within carbamoye phosphate synthetase. *J. Am. Chem. Soc.* **121,** 3803–3804
4. Knapp, M. J., Seebeck, F. P., and Klinman, J. P. (2001) Steric control of oxygenation regiochemistry in soybean lipoxygenase-1. *J. Am. Chem. Soc.* **123,** 2931–2932
5. Cohen, J., Kim, K., King, P., Seibert, M., and Schulten, K. (2005) Finding gas diffusion pathways in proteins: application to O2 and H2 transport in CpI [FeFe]-hydrogenase and the role of packing defects. *Structure* **13,** 1321–1329
6. Saam, J., Ivanov, I., Walther, M., Holzhutter, H. G., and Kuhn, H. (2007) Molecular dioxygen enters the active site of 12/15-lipoxygenase via dynamic oxygen access channels. *Proc. Natl. Acad. Sci. U.S.A.* **104,** 13319–13324
7. Johnson, B. J., Cohen, J., Welford, R. W., Pearson, A. R., Schulten, K., Klinman, J. P., and Wilmot, C. M. (2007) Exploring molecular oxygen pathways in *Hansenula polymorpha* copper-containing amine oxidas. *J. Biol. Chem.* **282,** 17767–17776
8. Leroux, F., Dementin, S., Burlat, B., Cournac, L., Volbeda, A., Champ, S., Martin, L., Guigliarelli, B., Bertrand, P., Fontecilla-Camps, J., Rousset, M., and Leger, C. (2008) Experimental approaches to kinetics of gas diffusion in hydrogenase. *Proc. Natl. Acad. Sci. U.S.A.* **105,** 1188–1193
9. Luna, V. M., Chen, Y., Fee, J. A., and Stout, C. D. (2008) Crystallographic

studies of Xe and Kr binding within the large internal cavity of cytochrome ba3 from *Thermus thermophilus*: structural analysis and role of oxygen transport channels in the heme-Cu oxidases. *Biochemistry* **47,** 4657–4665

10. Chen, L., Lyubimov, A. Y., Brammer, L., Vrielink, A., and Sampson, N. S. (2008) The binding and release of oxygen and hydrogen peroxide are directed by a hydrophobic tunnel in cholesterol oxidase. *Biochemistry* **47,** 5368–5377

11. Tomita, A., Sato, T., Ichiyanagi, K., Nozawa, S., Ichikawa, H., Chollet, M., Kawai, F., Park, S. Y., Tsuduki, T., Yamato, T., Koshihara, S. Y., and Adachi, S. (2009) Visualizing breathing motions of internal cavitiesin concert with ligand migration in myoglobin. *Proc. Natl. Acad. Sci. U.S.A.* **106,** 2612–2616

12. Dementin, S., Leroux, F., Cournac, L., de Lacey, A. L., Volbeda, A., Leger, C., Burlat, B., Martinez, N., Champ, S., Martin, L., Sanganas, O., Haumann, M., Fernandez, V. M., Guigliarelli, B., Fontecilla-Camps, J. C., and Rousset, M. (2009) Introduction of methionines in the gas channel makes [NiFe] hydrogenase aero-tolerant. *J. Am. Chem. Soc.* **131,** 10156–10164

13. Scorciapino, M. A., Robertazzi, A., Casu, M., Ruggerone, P., and Ceccarelli, M. (2009) Breathing motions of a respiratory protein revealed by molecular dynamics simulations. *J. Am. Chem. Soc.* **131,** 11825–11832

14. Saam, J., Rosini, E., Molla, G., Schulten, K., Pollegioni, L., and Ghisla, S. (2010) O2 reactivity of flavoproteins: dynamic access of dioxygen to the active site and role of a H$^+$ relay system in D-amino acid oxidase. *J. Biol. Chem.* **285,** 24439–24446

15. Song, W. J., Gucinski, G., Sazinsky, M. H., and Lippard, S. J. (2011) Tracking a defined route for O$_2$ migration in a dioxygen-activating diiron enzyme. *Proc. Natl. Acad. Sci. U.S.A.* **108,** 14795–14800

16. Winter, M. B., Herzik, M. A, Jr., Kuriyan, J., and Marletta, M. A. (2011) Tunnels modulate ligand flux in a heme nitric oxide/oxygen binding (H-NOX) domain. *Proc. Natl. Acad. Sci. U.S.A.* **108,** E881–E889

17. Wang, P. H., and Blumberger, J. (2012) Mechanistic insight into the blocking of CO diffusion in [NiFe]-hydrogenase mutants through multiscale simulation. *Proc. Natl. Acad. Sci. U.S.A.* **109,** 6399–6404

18. Minor, W., Steczko, J., Stec, B., Otwinowski, Z., Bolin, J. T., Walter, R., and Axelrod, B. (1996) Crystal structure of soybean lipoxygenase −1 at 1.4 A resolution. *Biochemistry* **35,** 10687–10701

19. Knapp, M. J., and Klinman, J. P. (2003) Kinetic studies of oxygen reactivity in soybean lipoxygenase-1. *Biochemistry* **42,** 11466–11475

20. Chovancova, E., Benes, P., Strnad, O., Brezovsky, J., Kozlikova, B., Gora, A., Sustr, V., Klvana, M., Medek, P., Biedermannova, L., Sochor, J., and Damborsky, J. (2012) CAVER 3.0: a tool for the analysis of transport pathways in dynamic protein structures. *PLoS Comput. Biol.* **8,** e1002708

21. Humphrey, W., Dalke, A., and Schulten, K. (1996) VMD: visual molecular dynamics. *J. Mol. Graphics* **14,** 33–38

22. Case, D. A., Darden, T. A., Cheatham, I. i. i., Simmerling, C. L., Wang, J., Duke, R. E., Luo, R., Walker, R. C., Zhank, W., and Merz, K. H. (2010) AMBER 11, University of California, San Francisco, p. 142

23. Jorgensen, W. L., Chandrasekhar, J., Madura, J. D., Impey, R. W., and Klein, M. L. (1983) Comparison of simple potential functions for simulating liquid water. *J. Chem. Phys.* **79,** 926–935

24. Giammona, D. A. (1984) *An Examination of Conformational Flexibility in*

Porphyrins and Bulky-ligand Binding in Myoglobin. Ph.D. thesis, University of California, Davis, CA

25. Wang, J., Cieplak, P., and Kollman, P. (2000) How well does a restrained electrostatic potential (RESP) model perform in calculating conformational energies of organic and biological molecules? *J. Comput. Chem.* **21,** 1049–1074

26. Hatcher, E., Soudackov, A. V., and Hammes-Schiffer, S. (2007) Proton-coupled electron transfer in soybean lipoxygenase: dynamical behavior and temperature dependence of kinetic isotope effects. *J. Am. Chem. Soc.* **129,** 187–196

27. Edwards, S. J., Soudackov, A. V., and Hammes-Schiffer, S. (2010) Impact of distal mutation on hydrogen transfer interface and substrate conformation in soybean lipoxygenase. *J. Phys. Chem. B* **114,** 6653–6660

28. Cohen, J., Olsen, K. W., and Schulten, K. (2008) Finding gas migration pathways in proteins using implicit ligand sampling. *Methods Enzymol.* **437,** 439–457

29. Rickert, K. W., and Klinman, J. P. (1999) Nature of hydrogen transfer in soybean lipoxygenase 1: separation of primary and secondary isotope effects. *Biochemistry* **38,** 12218–12228

30. Meyer, M. P., Tomchick, D. R., and Klinman, J. P. (2008) Enzyme structure and dynamics affect hydrogen tunneling: the impact of a remote side chain (I553) in soybean lipoxygenase-1. *Proc. Natl. Acad. Sci. U.S.A.* **105,** 1146–1151

31. Coffa, G., Schneider, C., and Brash, A. R. (2005) A comprehensive model ofpositional and stereo control in lipoxygenases. *Biochem. Biophys. Res. Commun.* **338,** 87–92

32. Hu, S., Sharma, S. C., Scouras, A. D., Soudackov, A. V., Carr, C. A. M., Hammes-Schiffer, S., Alber, T., and Klinman, J. P. (2014) Extremely elevated room-temperature kinetic isotope effects quantify the critical role of barrier width in enzymatic C–H activation. *J. Am. Chem. Soc.* **136,** 8157–8160

33. Berry, H., Debat, H., and Garde, V. L. (1998) Oxygen concentration determines regiospecificity in soybean lipoxygenase-1 reaction via a branched kinetic scheme. *J. Biol. Chem.* **273,** 2769–2776

34. Baron, R., Riley, C., Chenprakhon, P., Thotsaporn, K., Winter, R. T., Alfieri, A., Forneris, F., van Berkel, W. J., Chaiyen, P., Fraaije, M. W., Mattevi, A., and McCammon, J. A. (2009) Multiple pathways guide oxygen diffusion into flavoenzyme active sites. *Proc. Natl. Acad. Sci. U.S.A.* **106,** 10603–10608

35. Liebgott, P. P., Leroux, F., Burlat, B., Dementin, S., Baffert, C., Lautier, T., Fourmond, V., Ceccaldi, P., Cavazza, C., Meynial-Salles, I., Soucaille, P., Fontecilla-Camps, J. C., Guigliarelli, B., Bertrand, P., Rousset, M., and Leger, C. (2010) Relating diffusion along the substrate tunnel and oxygen sensitivity in hydrogenase. *Nat. Chem. Biol.* **6,** 63–70

36. Ivanov, I., Heydeck, D., Hofheinz, K., Roffeis, J., O'Donnell, V. B., Kuhn, H., and Walther, M. (2010) Molecular enzymology of lipoxygenases. *Arch. Biochem. Biophys.* **503,** 161–174

37. Glickman, M. H., and Klinman, J. P. (1996) Lipoxygenase reaction mechanism: demonstration that hydrogen abstraction from substrate precedes dioxygen binding during catalytic turnover. *Biochemistry* **35,** 12882–12892